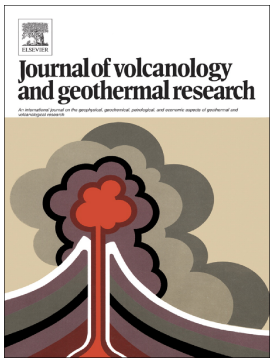

The seismic sequence of 30th May - 9th June 2016 in the geothermal site of Torre Alfina (central Italy) and related variations in soil gas emissions

Thomas Braun, Marco Caciagli, Maria Luisa Carapezza, Daniela Famiani, Alessandro Gattuso, Arianna Lisi, Alessandro Marchetti, Giuliana Mele, Nicola Mauro Pagliuca, Massimo Ranaldi, Francesco Sortino, Luca Tarchini, Marius Kriegerowski, Simone Cesca

PII: S0377-0273(18)30145-8
DOI: doi:10.1016/j.jvolgeores.2018.06.005
Reference: VOLGEO 6399

To appear in: *Journal of Volcanology and Geothermal Research*

Received date: 28 March 2018
Revised date: 18 May 2018
Accepted date: 4 June 2018

Please cite this article as: Thomas Braun, Marco Caciagli, Maria Luisa Carapezza, Daniela Famiani, Alessandro Gattuso, Arianna Lisi, Alessandro Marchetti, Giuliana Mele, Nicola Mauro Pagliuca, Massimo Ranaldi, Francesco Sortino, Luca Tarchini, Marius Kriegerowski, Simone Cesca , The seismic sequence of 30th May - 9th June 2016 in the geothermal site of Torre Alfina (central Italy) and related variations in soil gas emissions. Volgeo (2018), doi:10.1016/j.jvolgeores.2018.06.005

The seismic sequence of 30th May - 9th June 2016 in the geothermal site of Torre Alfina (central Italy) and related variations in soil gas emissions

Thomas Braun[a], Marco Caciagli[b], Maria Luisa Carapezza[c], Daniela Famiani[c], Alessandro Gattuso[c], Arianna Lisi[c], Alessandro Marchetti[d], Giuliana Mele[c], Nicola Mauro Pagliuca[c], Massimo Ranaldi[e], Francesco Sortino[c], Luca Tarchini[e], Marius Kriegerowski[f], Simone Cesca[f]

[a]*Istituto Nazionale di Geofisica e Vulcanologia, Osservatorio di Arezzo (IT)*
[b]*Istituto Nazionale di Geofisica e Vulcanologia, Bologna (IT)*
[c]*Istituto Nazionale di Geofisica e Vulcanologia, Sezione di Roma (IT)*
[d]*Istituto Nazionale di Geofisica e Vulcanologia, Centro Nazionale Terremoti, Roma (IT)*
[e]*Dipartimento di Scienze, Universitá di Roma Tre, Roma, (IT)*
[f]*Geoforschungszentrum-Potsdam, Potsdam (DE)*

Abstract

In the framework of a medium-enthalpy geothermal exploitation project, seismicity and soil gas emissions have been monitored in the area of Castel Giorgio - Torre Alfina (central Italy) since 2014. A dedicated local seismic network, called ReMoTA, allows deepening of the knowledge of the natural local seismicity in terms of source mechanisms, high-quality event localization and magnitude estimation. From November 2014 to May 2016, ReMoTA recorded 846 seismic events with a magnitude range of M_d 0.1 to M_L 2.8 and with hypocentres between 4 and 8 km depth. Most of these events occurred in six short lasting clusters. On 30th May 2016 a M_w 4.3 earthquake occurred near Castel Giorgio, followed by almost 1700 aftershocks. The moment tensor solution for the main shock depicts a WNW-ESE oriented normal fault with small right-lateral strike component. An overview of the epicentral distribution of the different clusters recorded since 2014, highlights that the active tectonic structures are orientated principally along the NE - SW and WNW-ESE directions. The relocation of the 1957 M_e 4.9 historical earthquake suggests that this event occurred in the same fault system as the 2016 seismic sequence. In the study area, there is only one natural emergence (Solfanare) emitting a CO_2 dominated gas, having the same

chemical and isotopic composition of the gas contained in a cap at the summit of the geothermal reservoir. Apart from small perturbations, no significant compositional variations, were recorded during the 2016 seismic sequence in the gas of the Solfanare vents that was also analyzed continuously by an automatic gas-chromatographic station. The diffuse soil CO_2 flux is monitored since 2013 in six target areas located around the future production and reinjection wells, in order to assess the level of background natural degassing. In all target areas the maximum value of soil CO_2 flux has been recorded during the 2016 seismic sequence. However, values remained relatively low (maximum 112 $g \cdot m^{-2} \cdot d^{-1}$) and the values of $\delta^{13}C$ of the emitted CO_2 (-25.25 to -24.22 ‰ vs. PDB) indicated a shallow biological origin of the gas (by soil respiration). Only at Solfanare high values of diffuse soil CO_2 flux were recorded up to a maximum of $20,125$ $g \cdot m^{-2} \cdot d^{-1}$). All the seismicity of the May - June 2016 sequence is located above the M_L4.1 main event and is distributed on small distinct faults (such as at San Lorenzo Nuovo, Acquapendente, etc.) and triggered by the main shock. The source mechanism provided by the full moment tensor indicates that rupture processes at depth probably deviate from a pure normal fault. The significant contribution of CLVD and isotropic components suggest a possible opening of fluid cracks below the geothermal reservoir hosted in fractured Mesozoic limestones. In spite of the increase of the CO_2 flux, no significant changes have been observed in the chemical and isotopic composition of the *Solfanare* gas. The seismo-tectonic scenario indicates that the *Solfanare* fault was not activated. Kinematics and orientation of the activated faults suggest a relationship with the Bolsena caldera collapse.

Keywords: Local Seismicity, Soil Gas Emissions, Geothermal Exploration, Torre Alfina, Central Italy

2017 MSC: 00-01, 99-00

1. Introduction

Apart from Iceland and Greece, the main high-temperature geothermal areas of Europe are situated in Italy (Batini et al., 1980a,b, 1985, 1990; Evans et al., 2012; Moia et al., 1993; Mucciarelli et al., 2001; Cesca et al., 2013; Braun et al., 2018). The entire Italian high-enthalpy geothermal energy is produced in central Italy, at the power plants of Larderello and Mt. Amiata (e.g. Braun et al., 2016, and references therein). Upcoming geothermal exploitation now focuses, among others, on the area of Torre Alfina - Castel Giorgio, located at the boundary between the regions of Tuscany and Latium (Figure 1). Here, a private industrial company applied for the permit of developing two geothermal pilot plants, each with a capacity of 5 MWe. A numerical model of fluid circulation within the geothermal reservoir by Volpi et al. (2018) supports the sustainability of such a production. Thereupon, the Istituto Nazionale di Geofisica e Vulcanologia (INGV) was commissioned, in 2013, to realize a multi-parametric system for the monitoring of soil gas emissions, microseismicity and in future also for ground deformation (Carapezza et al., 2015; Braun et al., 2017).

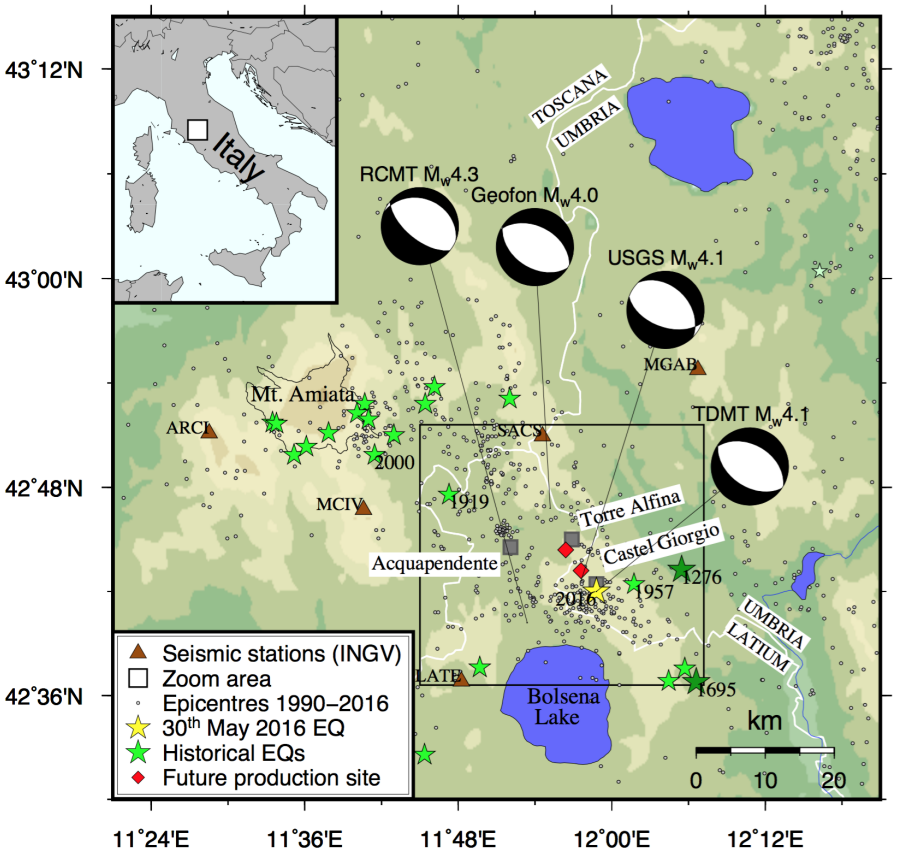

Figure 1: Map of the study area showing the seismicity from 1990 - 2016 (ISIDe working group, 2016), the historical seismicity (Locati et al., 2016) and the INGV seismic network. The black rectangle refers to the area zoomed in Figure 3. Black lines show the different locations of the 30th May 2016 main shock and the beachballs their respective moment tensors proposed by CNT-TDMT (Scognamiglio et al., 2009), RCMT (Pondrelli et al., 2006), GEOFON (http://geofon.gfz-potsdam.de), USGS (Herrmann et al., 2011).

The historical seismicity of the geothermal area between Mt. Amiata and the Bolsena lake can be considered as "moderate". As shown in Figure 1, the Parametric Catalogue of Italian Earthquakes (CPTI) (Locati et al., 2016) reports 21 earthquakes since 1000 A.D. with $I_o \geq$ VI and estimated as "equivalent magnitude" M_e 5.8. The strongest earthquakes are the M_e 5.8 (1695) that struck the area east of the Bolsena lake, and the M_e 5.6 (1276) that occurred near Orvieto.

According to the CPTI, the only earthquakes that damaged the villages of Torre Alfina and Castel Giorgio in historical times are those of 1919 (M_e 5.3), near Mt. Amiata, and 1957 (M_e 4.9), near Castel Giorgio. Recent seismic sequences, as the one in May 2016, described in this work, testifies a continuous stress relaxation through earthquakes.

This contribution presents:

(i) a general description of the geothermal field and of the recently installed seismic network ReMoTA;

(ii) a detailed description of the seismic sequence started on 30^{th} May 2016;

(iii) an estimate of the source parameters obtained by comparing moment tensors with focal mechanisms computed from first motion polarities;

(iv) the results of the geochemical monitoring of soil gas emissions;

(v) the relocation of the M_e 4.9 (1957) earthquake occurred near Castel Giorgio, based on historical instrumental data;

(vi) an empirical relationship for the local magnitude M_L;

(vii) a discussion about the relationship between the seismo-tectonic setting and the geothermal area.

2. The geothermal reservoir of Torre Alfina

The geothermal area of Torre Alfina - Castel Giorgio is located in central Italy, at the northern extremity of the Quaternary Vulsini volcanic complex.

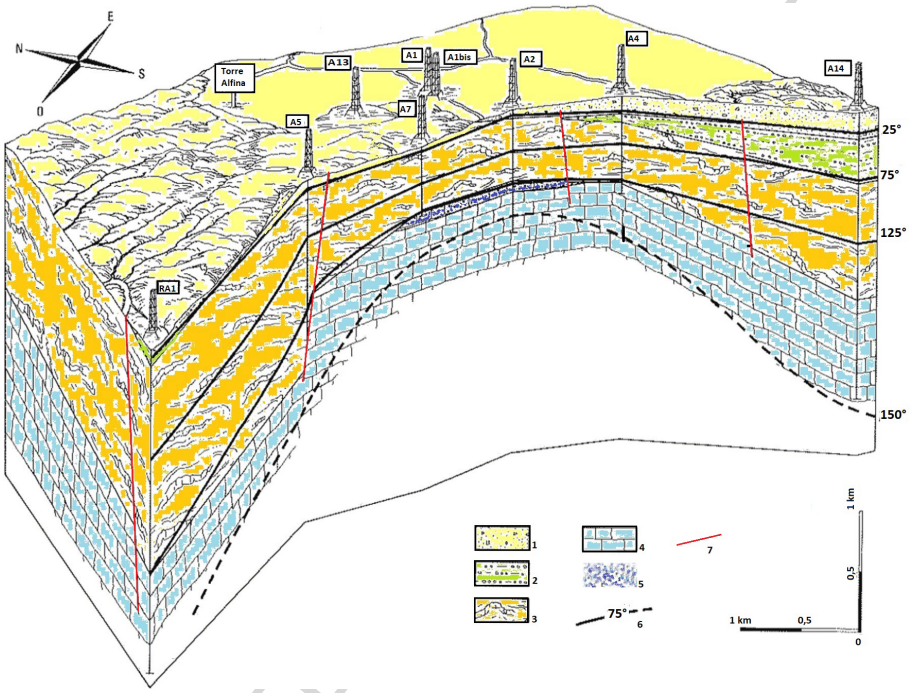

Figure 2: Schematic block diagram of the Torre Alfina geothermal field derived from deep drilling data. (1) Quaternary volcanic deposits (2) Pliocene marine deposits (3) allochthonous Ligurian flysch (4) Mesozoic fractured limestones hosting the geothermal reservoir (5) extent of the gas cap in the central part of the field (6) isotherms in °C; (7) normal faults (modified after Buonasorte et al., 1988).

Exploration wells drilled in the 1970s and 1980s down to depths ranging from 563 to 2,710 m (Figure 2) revealed that Torre Alfina is a medium-enthalpy (T = 140°C) geothermal field, hosted in fractured Mesozoic limestones of the Tuscan series (Buonasorte et al., 1988). The geothermal reservoir is hosted inside a buried horst; its top was drilled at a minimum depth of 550 - 650 m below the ground surface (Figure 2). At the summit of the reservoir is a gas cap,

which has been extensively exploited for CO_2 production (Carapezza et al., 2015, and references therein). The geothermal fluid is hot water with a dissolved salt content of about 5,000 ppm and about 2 wgt.% of dissolved CO_2. The reservoir cover is made of allochthonous Ligurian flysch and overlying Neogenic shales. The Quaternary surface volcanic rocks host a cold aquifer.

A deep exploration well (4,826 m) was drilled in the late 1980s in search for a deeper and hotter geothermal reservoir inside the Triassic-Paleozoic metamorphic formation, as that existing in the Tuscan geothermal fields of Larderello and Mt. Amiata. However, the well crossed a thick sequence of thrusted limestones of the Tuscan series covering thrusted limestones of the Umbrian series without reaching the metamorphic basement (Buonasorte et al., 1991).

In the geothermal area of Torre Alfina, the only natural gas manifestation, called *Solfanare*, is located about 1 km SSE of the Torre Alfina village; here, a cold gas is emitted from a NNW - SSE fault, with the same composition as the one contained in the reservoir gas cap (Carapezza et al., 2015).

3. ReMoTA - the INGV seismic network installed at Torre Alfina

As mentioned, the INGV was charged of realizing a multi-parametric monitoring system in the area of the future production sites following the guidelines, published by the Italian Ministry of Economic Development (MISE) in 2014 (called ILG-2014, hereafter, Dialuce et al., 2014). The ILG-2014 describe in detail the governmental regulations, especially regarding hydrocarbon extraction, of waste-water injection, and CO_2 storage. A more recent edition of the ILG, concerning the geothermal energy production, was issued in 2016 (ILG-2016, hereafter Terlizzese, 2016); both versions of the guidelines prescribe the monitoring of pore pressure, microseismicity and ground deformation.

While the ILG-2014 define two monitoring areas called "Internal Domain" (DI) and "External Domain" (DE), with a radius of 5 and 10 km, respectively, around the reinjection sites, the ILG-2016 define the boundaries of these areas as 2 and 7 km from the bottom of the reinjection wells.

In a three-years test phase, the ILG will be applied in 4 experimental areas:

(i) Val d'Agri (Basilicata, southern Italy) and

(ii) Cavone (Emilia Romagna, northern Italy) for hydrocarbon exploitation, including waste water reinjection;

(iii) Minerbio (Emilia Romagna) for gas storage;

(iv) Casaglia (Emilia Romagna) for low-enthalpy geothermal production.

Before starting new exploitations, industrial companies are requested to provide an environmental impact assessment (EIA) that has to include also the monitoring of the natural seismicity in the future production area, for at least 12 months before the beginning of the exploitation.

Following the ILG-2014, our 10 stations seismic network ReMoTA is in its final configuration (Figure 3), fulfilling already the EIA requirements.

All seismic stations are equipped with a 24-bit digitizer and a short-period seismometer, except station TA06 where a broadband seismic sensor is installed. To select the final installation sites, intensive seismic noise studies have been carried out, which revealed a moderate quality for most station sites. As described in detail by Braun et al. (2017), electrical generators, pumps etc., driven by local industries generate noise in the frequency bands 1.5 - 2 Hz and 3.5 - 4 Hz, traveling through all the DI-stations, as well as local monochromatic signals between 8 and 15 Hz, depending on the station site and recording period.

Considering that small local earthquakes radiate seismic energy in the higher frequency bands, the disturbances at 1.5 - 2 Hz do not influence significantly the detection capabilities of ReMoTA (Braun et al., 2017; Lisi et al., 2018). While the monochromatic noise above 8 Hz can be suppressed by applying notch-filtering, noise around 4 Hz blurs the spectral energy radiated by local seismic events in this frequency band, lowering the detection capabilities of ReMoTA.

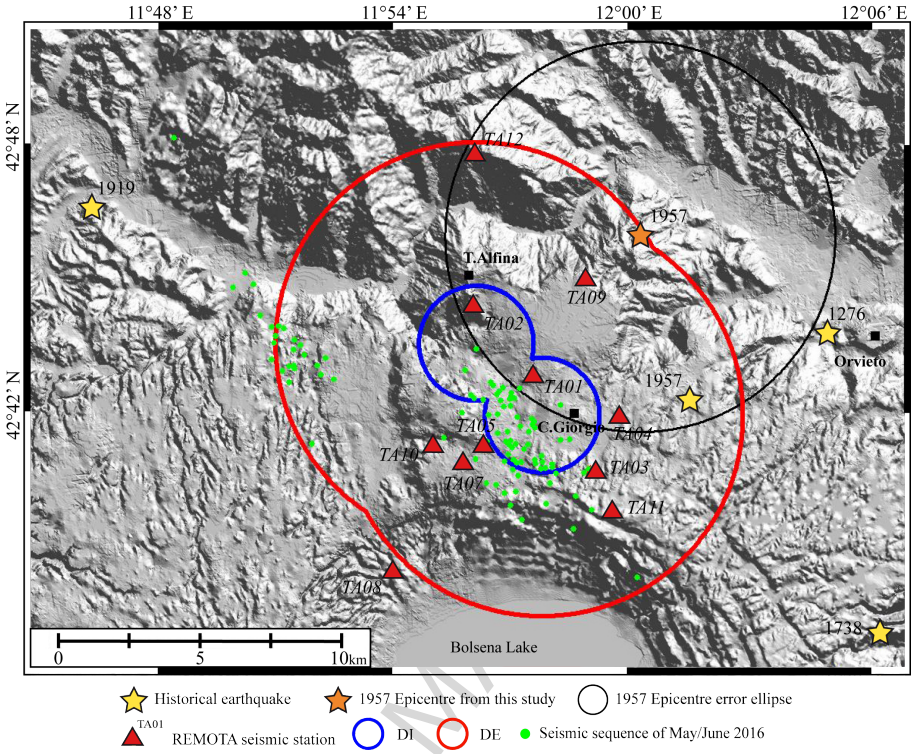

Figure 3: Shaded relief map showing the ReMoTA seismic network and the Internal (blue) and External (red) Domains defined in the ILG-2016. The epicentre of the seismic sequence of May - June 2016 (green dots) reported by ISIDe working group (2016) and of the historical 1276, 1919 and 1957 earthquakes (yellow stars from Locati et al., 2016) are also shown. The orange star indicates the recalculated epicentre of the 6th December 1957 earthquake along with the corresponding error ellipse (black circle).

4. Analysis of the seismic sequence of 30th May 2016

4.1. Temporal evolution of the seismic sequence

The seismic sequence started on 30th May 2016 at 20:24:21 UTC (Universal Time Code) with an earthquake of M_L 4.1 and was followed by more than 1,600 aftershocks, three of them with magnitude of $M_L \geq 3$ (Table 1). The strongest of these aftershocks (M_L 3.4) occurred near Acquapendente, 10 km NW with respect to the main shock. In this paper, we analyze the seismic sequence and the following background seismicity until the end of 2016.

Panel	Date	Origin time	Lat.	Long.	Depth	Mag.
Fig. 4	yyyy-mm-dd	hh:mm:ss.ms	°N	°E	*km*	M_L
(d)	2016-05-30	20:24:21.000	42.71188	11.96610	6.94 km	4.1
(e)	2016-05-31	09:22:32.060	42.74974	11.87848	4.62 km	3.4
(f)	2016-05-31	20:31:30.940	42.71082	11.95749	5.79 km	3.0
(g)	2016-06-02	03:27:01.390	42.70925	11.96274	5.88 km	3.2

Table 1: Panel in Figure 4, origin times (UTC) and hypocentres of the strongest events ($M_L \geq 3$) of the 2016 sequence.

We manually picked the P- and S-wave arrival times recorded by the ReMoTA temporary stations and by the INGV permanent stations SACS, LATE, MGAB and MCIV (locations in Figure 1). For the strongest earthquakes, we added the P- and S-phase readings of the INGV Seismic Bulletin. A total of 1,831 events were located using the Hypoellipse code (Lahr, 1999) and a velocity model (Table 2) obtained merging the model of Chiarabba et al. (1995) for the first 7 km with that used by the INGV (Mele et al., 2010) for the deeper layers. The model by Chiarabba et al. (1995) was calculated from a high-resolution tomography based on the inversion of 7,535 P- and 563 S-wave arrival times of 676 earthquakes occurred in the Torre Alfina area and in the geothermal fields of Torre Alfina, Latera and Mt Amiata; the associated v_p/v_s ratio was 1.79.

Depth	V_p	V_s
km	km/s	km/s
0.00	3.00	1.68
1.10	4.55	2.54
3.00	5.12	2.86
5.00	5.83	3.26
7.00	6.41	3.58
11.00	6.50	3.63
38.00	8.05	4.50

Table 2: Crustal 1D-velocity model used for the relocation (after Chiarabba et al., 1995).

We recomputed the average local v_p/v_s ratio, applying the modified Wadati method (Chatelain, 1978; Pontoise and Monfret, 2004). The linear fit of the time difference between the P and S phases (ΔT_p and ΔT_s) for the available station pairs gives a v_p/v_s ratio of 1.817 within a confidence of 95%, a root-mean squares (RMS) error of 0.0197, and a linear coefficient of R= 0.84 (see electronic supplement ES-Figure 15). We then applied the double-difference (DD) location algorithm HypoDD (Waldhauser and Ellsworth, 2000; Waldhauser, 2001) to improve the hypocentral determination (Figure 4).

Hypocentres result in a depth range between 2 and 8 km (the distribution of horizontal and vertical errors, and the RMS for the relocated earthquakes are shown in ES-Figure 16). For the period from 30th May to 14th June, we located 1670 seismic events; 1598 in an area of Castel Giorgio, 72 around Acquapendente, and further 135 earthquakes until the end of 2016. During the sequence, the seismicity mainly concentrated in the first four days (see ES-Figure 17), and started to decrease soon after the occurrence of the M_L 3.2 event (g in Table 1, Figure 4). Analyzing in detail the sequence, we found that during the first 15 hours after the main shock, 865 earthquakes occurred along different tectonic structures located close to Castel Giorgio, Acquapendente and San Lorenzo Nuovo. The main seismic activity is mainly concentrated northwest

to Castel Giorgio and depth increase southeastward down to 7 km (Figure 4). Contrary, the hypocentral depth of the seismicity near Acquapendente (location of the M_L 3.4 event, Table 1) increase northeastward down to 7 km also (Figure 4). The smaller clusters, such as San Lorenzo Nuovo, show a more vertical distribution and shallower hypocentral depth between 4 and 5 km.

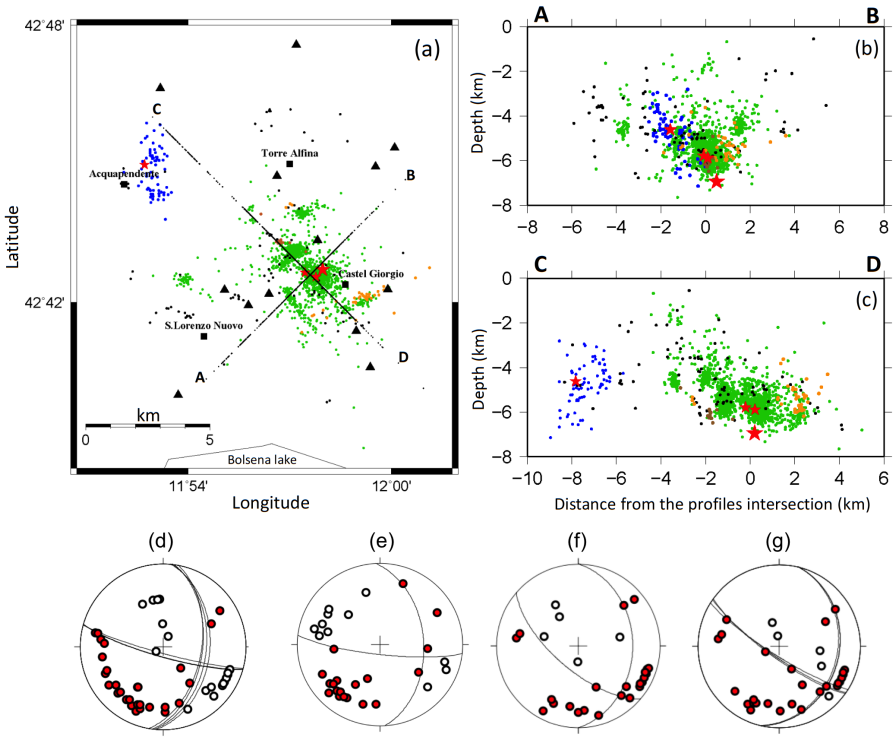

Figure 4: Map (a) and sections (b)(c) of the seismicity from 30th May to 31st December 2016. The green and the blue dots indicate the location of the earthquakes occurred during the sequence from 30th May to 15th June; the red stars indicate the main shock and the aftershocks with M $\geq$ 3. The black dots show the background seismicity from 15th June to the end of 2016, while the orange and brown dots are related to a small cluster consisting of 36 events recorded from 9th to 10th of July and in 13 earthquakes occurred on 16th October, respectively. The black triangles show the ReMoTa local network. Focal mechanisms of the four (d),(e),(f),(g) strongest events (see Table 1) were calculated using first motion polarities and the local velocity model (Table 2).

Then, in the following three days, from 31st May (12:00 UTC) to 3rd June (12:00 UTC), we recorded 628 events concentrated mainly in an area closer to Castel Giorgio. Furthermore, during these three days, seismicity migrated from NW to SE. The hypocentral depth is between 5 and 7 km, slightly deeper than that of the previous shocks (Figures 4. The cluster close to Acquapendente (Figure 4) started on 30th May as the sequence in Castel Giorgio, lasted 4 days and consisted of 72 earthquakes. The epicenters are distributed along a N - S direction, and the hypocenters become deeper towards N - NE reaching a maximum depth of about 7 km (Figure 4).

4.2. Moment tensor of the main shock

The moment tensor (MT) of the main shock was calculated using local to regional broadband INGV stations located at 25 - 100 km distance from the epicentre. Following the methodology described by Cesca et al. (2010, 2013), the inversion consists in fitting both the 3-components full waveform amplitude spectra and the full waveform displacements, bandpass filtered between 0.02 and 0.10 Hz.

The best MT solution is found for a hypocentral depth of 5 km, with a dominant normal faulting component oriented NW-SE (strike 101/311, dip 46/48, rake -111/-69), and marginal positive isotropic and positive CLVD components. The double couple (DC) solution (strike 128/304, dip 45/34, rake -87/-93; red contour on beachball in Figure 5) changes in orientation for depths larger than 7 km, but it is associated to a worse fit.

The non-DC term characterization is observed also for variable depths. The seismic moment is $3.53 \cdot 10^{15}$ Nm, corresponding to a moment magnitude of M_w 4.3.

This result is coherent with the regional moment tensors shown in Figure 1, which unanimously found for the main shock of 30th May 2016 a clear normal fault mechanism with an Apenninic (NW - SE) strike direction (all assuming a standard depth of 5 km and a standard Earth model).

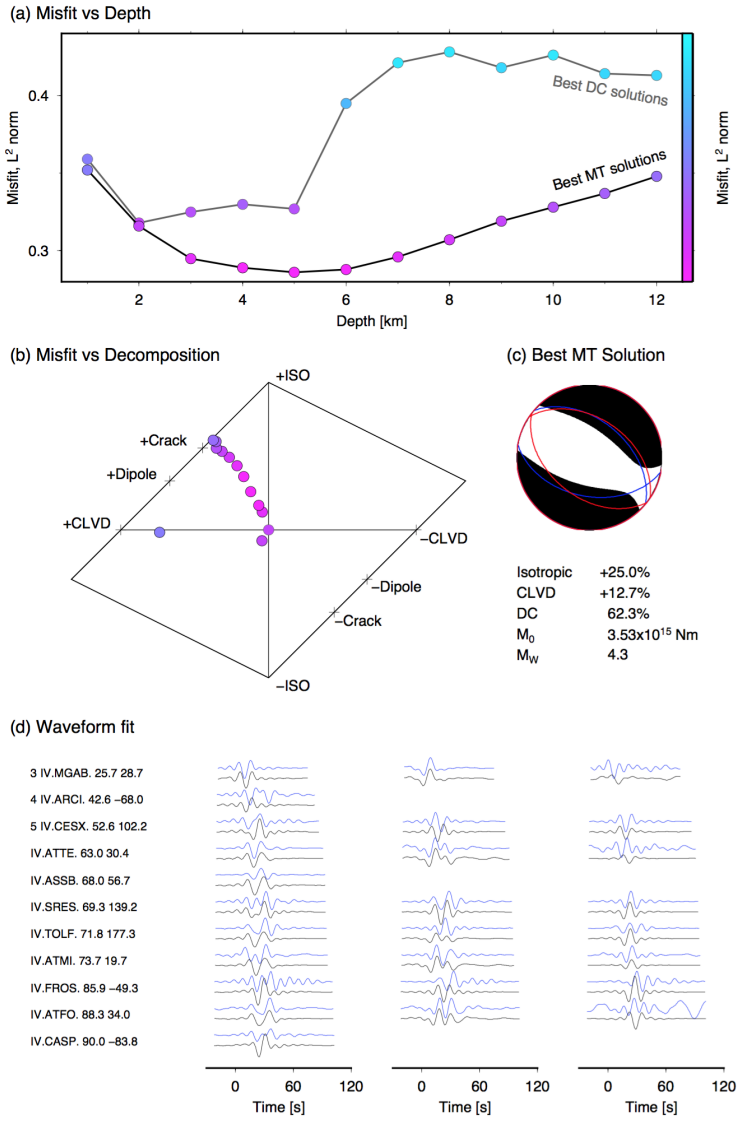

Figure 5: Summary of the moment tensor inversion results of the 30th May 2016 main shock computed using waveforms within 100 km of epicentral distance. (a) misfit vs. depth, assuming a DC source model (gray line) and full MT model (black line); (b) source-type diagram according to Hudson et al. (1989); (c) summary of the best modelling MT solution (black beachball); blue and red lines indicate the focal mechanisms of the DC component of the full MT solution and the pure DC solution, respectively; (d) comparison of normalized displacement waveform fits (real data in blue, synthetic in blacks); station, epicentral distance (in km) and azimuth (in degrees).

4.3. Depth phase of the main shock

To verify the hypocentral depth of the main shock, we used an alternative method and an independent dataset taken from the Canadian seismic array Yellowknife (YKA), situated at teleseismic distance. We compared the synthetic array beam with the beam-trace of the recorded array data. For this purpose, synthetic YKA-array beams have been generated for different source depths, varying from 1 to 14 km (black traces in Figure 6), using the predominant source mechanism reported by GEOFON (Figure 1) and the CRUST2 profile for Torre Alfina.

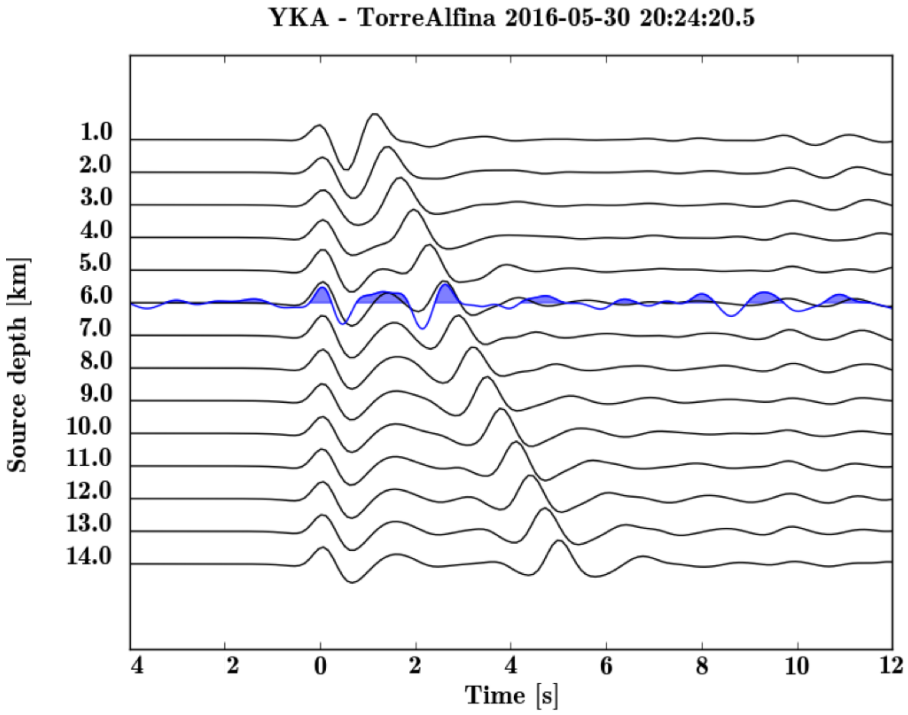

Figure 6: Array beam modelling of the 30th May 2016 main shock (M_w 4.3) computed using the Yellowknife-Array (YKA): the array beam (blue trace) is plotted with respect to theoretical velocity seismograms, calculated for different depths (black traces).

The advantage of this approach is that we can isolate direct P and surface reflected pP phases which follow a common ray path, except at the source region, where the pP phase samples the shallow crustal structure, between hypocentral depth and free surface. Using a dense array, we can improve the signal-to-noise ratio and observe a clean seismic signal at teleseismic distances.

The theoretical lag times between direct (P) and depth phases (pP) $\Delta(t_p - t_{pP})$ have then been compared with those of the beam-trace recorded at YKA. Figure 6 shows that the beam modelling at the YKA array provides the best fit of P - pP phases at a depth of about 6 km, both for velocities and displacements.

4.4. Magnitudes

For the calculation of the local magnitude reported in ISIDe working group (2016), the Seismic Monitoring Center of the ISN uses generally a formula by Hutton and Boore (1987), proposed originally for California:

$$M_L = log(A_0) + 1.11 \cdot log(r/100) + 0.00189 \cdot (r - 100) + 3.0 \qquad (1)$$

where $\log(A_0)$ is the half of the peak-to-peak amplitude of the corresponding Wood-Anderson (WA) seismogram [in mm] and r is the station-to-source-distance [in km]. To avoid the introduction of errors for the magnitude calculation at each single seismic station due to the non-consideration of the focal depth, only seismograms recorded in a distance range of 10 km $\leq$ r $\leq$ 600 km have been considered (as described by Arcoraci et al., 2012).

During the May-June 2016 seismic sequence near Castel Giorgio the epicentral distances of the ReMoTA-stations were comparable or less than the corresponding hypocentral depths, such that the above mentioned equation 1 could not be applied for the calculation of M_L. To calibrate the local magnitude of the ReMoTA recordings, we therefore chose the following approach:

we selected from the 1689 events, comprising ReMoTA catalog, those 98 earthquakes reported also by ISIDe working group (2016) for the period from 30^{th} May to 20^{th} June 2016, and calculated M_L using different established local magnitude formulas. We selected therefore five of the nine ReMoTA stations,

equipped with the same instrumentation, and calculated the horizontal WA displacement amplitudes. We calculated then M_L(ReMoTA) by using equation 1 and different local magnitude formulas. The first approach was to use the same equation used by the seismic monitoring center of ISN (equation 1), followed by recently published magnitude relations including the Gutenberg and Richter (1954) formula.

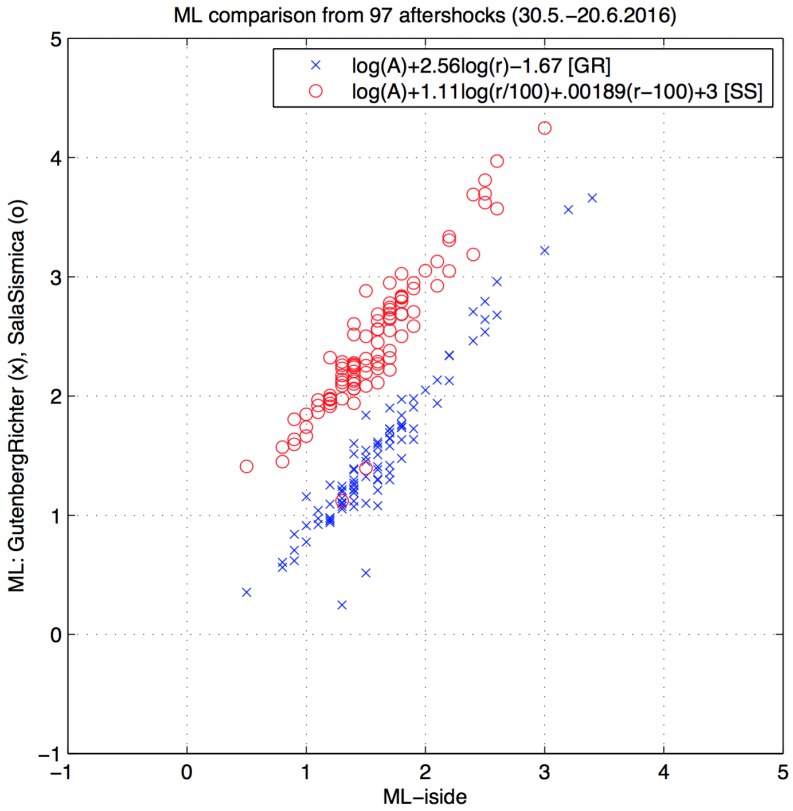

Figure 7: Comparison of local magnitudes from 98 events (30^{th} May - 20^{th} June 2016) recorded by ISN and ReMoTA: M_L-iside (reported by ISIDe working group, 2016) (red circles) are plotted with respect to M_L (after Gutenberg and Richter, 1954) (blue x), using the horizontal WA-amplitudes recorded by ReMoTA.

Figure 7 shows the fitting relation between M_L(ReMoTA) and M_L(ISIDe) that is surprisingly not given by the Hutton and Boore (1987) equation (red

circles), used by the ISN (Arcoraci et al., 2012), but provided by the original Gutenberg and Richter (1954) formula (blue x in Figure 7):

$$M_L = log(A_0) + 2.56 \cdot log(r) - 1.67 \quad (2)$$

where the epicentral distance r was replaced by the hypocentral distance.

5. Geochemical observations

5.1. Composition of the natural gas emissions

The *Solfanare* is the only natural gas emission site in the Torre Alfina geothermal area (Carapezza et al., 2015). It is characterized by many gas bubbling points that dry up during summer, leaving small emission vents. The water in the bubbling pools has a low temperature, with seasonal changes ($10.5 - 18.0^{o}$ C), very low pH (2.95 - 3.38), low salinity (TDS < 400) and a Ca+Mg sulphate composition due to the oxidation of H_2S from the bubbling gas in a shallow circulating water (Duchi et al., 1987). The anomalous P_{CO_2} and NH_4/B ratio confirms that the water composition is modified by a geothermal input.

The gas of the *Solfanare* emissions has the same chemical and isotopic composition of the gas sampled from the TA13 well tapping the gas cap at the top of the carbonate geothermal reservoir (Table 3 and Carapezza et al., 2015). As discussed by Carapezza et al. (2015), this gas has a low helium isotopic composition (R/Ra= 0.36 - 0.41), similar to that found in the fluid inclusions of the associated volcanic rocks, which is typical of all central Italy gas emissions (Martelli et al., 2004). This suggests that natural and geothermal gases have a significant component of deep magmatic or metasomatised mantle origin. Such an origin is compatible with the isotopic composition (δ^{13}C) of the CO_2 carbon (1.2 - 1.3 ‰ vs. PDB).

The *Solfanare* gas has been re-sampled during the seismic sequence, on 1st, 5th and 6th June 2016. Chemical and isotopic data are compared in Table 3 with previous data. It is clear from Table 3 that no significant chemical changes

have occurred in the *Solfanare* gas during the 2016 seismic sequence, and also the $\delta^{13}C$ composition of CO_2 and CH_4 remained the same of the gas emitted before the main shock.

The chemical composition of the *Solfanare* gas was also continuously monitored by an automatic gas chromatography monitoring station (CMS) (see Figure 8 for location). The CMS is a Micro Gas Chromatograph (μGC) equipped with two chromatographic modules (with poraplot and molecular sieve), each containing an injector, a chromatographic column and a micro thermal conductivity detector (TCD). At *Solfanare*, the gas was aspirated from the sampling point at 50 cm depth in the soil by an external pump through a Rilsan pipe with an internal diameter of 3 mm. Argon was used as gas carrier. Data were recorded at INGV, through an internet connected PC. The CMS was installed on 3rd June 2016 at 17:52 (UTC) and up to 6th June 01:47 it operated discontinuously with an analytical frequency of 5 min. Then it operated regularly from 6th June 14:27 to 21st June 2016 11:26, with a 30 min analytical frequency.

The temporal variation of the CO_2 concentrations (recalculated to 100%) and of the CO_2/H_2S, CO_2/CH_4, CO_2/H_2 concentration ratios in the *Solfanare* gas, recorded by the automatic CMS, is reported in Figure 9. During the last part of the seismic sequence from 3rd - 13th June 2016, CO_2 concentration showed some minor fluctuations, up to $\pm$ 0.2%, mostly with lower values but also with some higher ones, with respect to its average concentrations of 98.89%. After the seismic sequence these concentration fluctuations ceased and CO_2 values showed only a minor diurnal variation (Figure 9).

It is evident from Figure 9 that during the seismic sequence CO_2/H_2S, CO_2/CH_4 and CO_2/H_2 ratios showed relatively high fluctuations reaching their maximum values and then, more or less rapidly, they turned to steady-state values, also showing minor day-night variations controlled by environmental parameters. Therefore, data indicate that during the seismic sequence the concentrations of the reduced species reached their minimum values, likely because of an oxidation process occurred during the seismic soil shaking. In any case, there is no geochemical evidence of an increasing uprise of deep originated gas

(from the geothermal reservoir) caused by the 2016 earthquake.

Sample	Date	He	H_2	N_2	O_2	CH_4	CO_2	H_2S	^{40}Ar	$^4He/^{20}Ne$	R/Ra	$\delta^{13}CCO_2$	$\delta^{13}CCH_4$
	$d-m-y$	*ppm*	*ppm*	%	%	%	%	*ppm*	*ppm*			‰ vs. PDB	‰ vs. PDB
Geothermal well													
TA13[a]	10-11-1999	4.0	96	1.0	-	0.20	98.8	-	-	40.0	0.41	1.3	-
Solfanare													
natural emissions													
TAS4[b]	1-8-2012	7.0	247	0.84	0.16	0.16	98.43	700*	-	-	-	-	-
TA A[b]	23-4-2013	5.34	-	-	-	-	-	650*	-	21.6	0.37	1.3	-
TA A[b]	25-9-2013	5.01	bdl	1.2	0.14	0.15	97.8	730*	88.9	27.2	0.36	1.2	-21
TA B[b]	25-9-2013	4.96	bdl	0.9	0.05	0.15	98.3	750*	39.0	32.0	0.36	-	-
TA M[c]	1-6-2016	6.0	-	1.45	0.19	0.16	96.59	232	-	-	-	1.43	-21.43
TAS1[c]	1-6-2016	5.0	-	1.29	0.13	0.16	96.63	261	-	-	-	1.22	-
TA B[c]	1-6-2016	5.0	-	1.59	0.21	0.15	96.15	352	-	-	-	1.42	-
TA M[c]	5-6-2016	5.0	-	1.95	0.30	0.16	96.04	464	-	-	-	-	-
TAS1[c]	5-6-2016	5.0	-	1.13	0.08	0.16	96.88	490	-	-	-	-	-
TA B[c]	5-6-2016	5.0	-	1.50	0.19	0.16	96.82	535	-	-	-	-	-
TA M[c]	6-6-2016	5.0	-	1.41	0.15	0.16	96.54	279	-	-	-	-	-
Soil gas in		CO_2 flux					CO_2 %				$\delta^{13}CCO_2$		
target areas		g/m^2day					at 50 cm depth				‰ vs. PDB		
A4 1[c]	9-6-2016	82.3					5.20				-25.27		
A4 2[c]	9-6-2016	77.0					5.06				-24.22		

Table 3: Chemical and isotopic composition of Torre Alfina gas emissions. Source of data: [a] Martelli (2002), [b] Carapezza et al. (2015), [c] this work, * measured in the field with Draeger XAM-7000

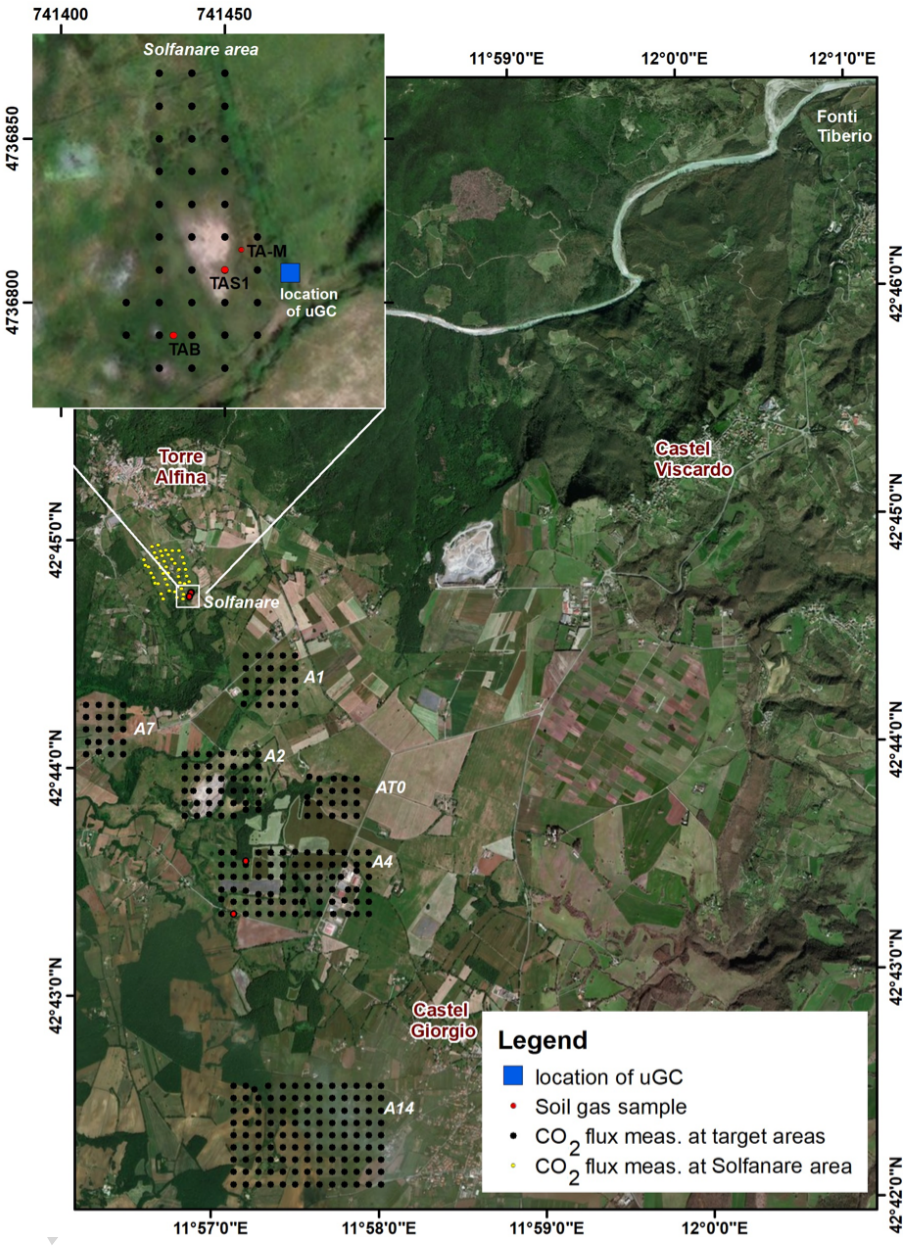

Figure 8: Geochemical monitoring of the geothermal area of Torre Alfina-Castel Giorgio: gas sampling sites (red dots) and location of the target areas (A1, A2, A4, A7, A14, AT0) and of the *Solfanare* area (magnified box) monitored for soil CO_2 flux.

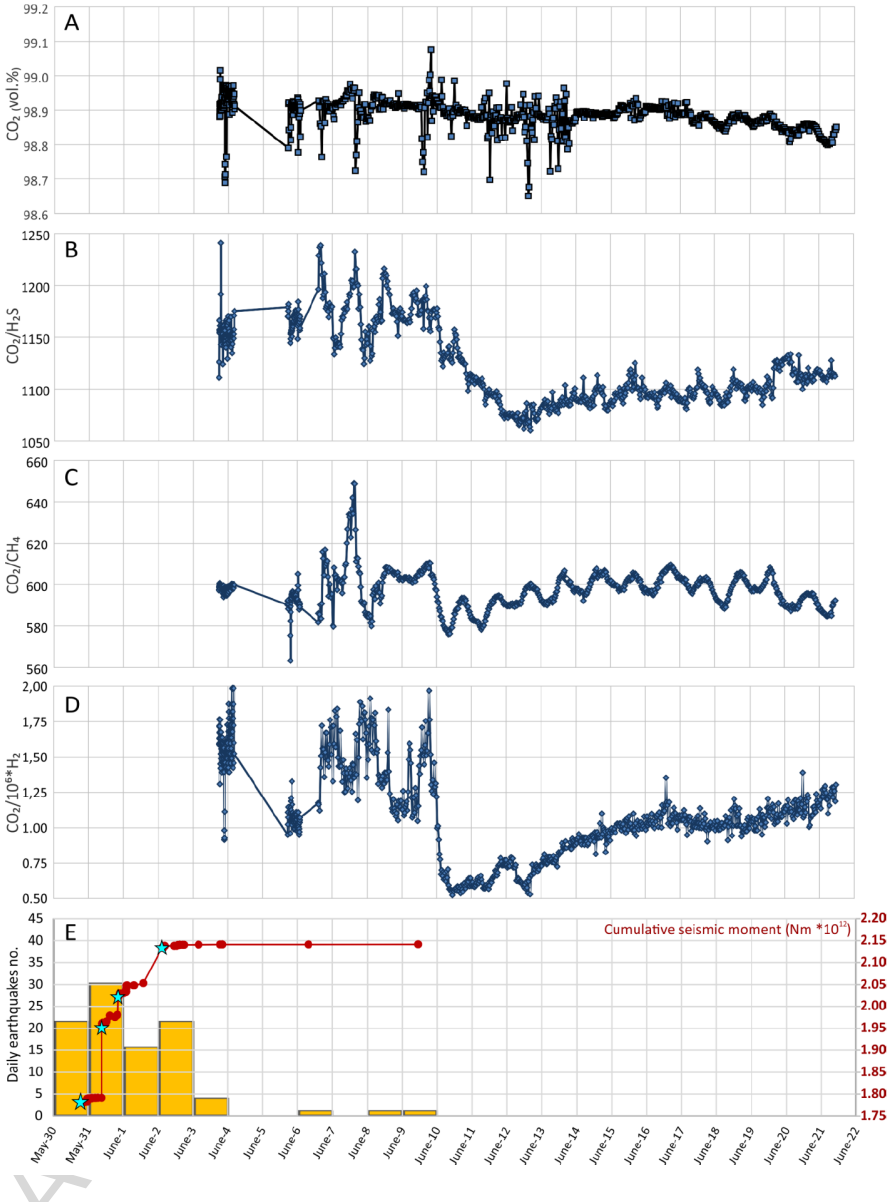

Figure 9: Temporal variation of (A) CO_2 concentration, (B) CO_2/H_2S ratio, (C) CO_2/CH_4S ratio, (D) $CO_2/10^6*H_2$ ratio, measured in 2016 by the automatic CMS in the Solfanare soil gas, (E) daily number of earthquakes (yellow bar, left axis) with the cumulative seismic moment (red circles and line, right axis) recorded during the 2016 sequence, reported by ISIDe working group (2016). The four main seismic events are indicated by a cyan star.

5.2. Soil CO_2 flux

Carbon dioxide is, after steam, the main volatile released from the geothermal systems of medium-high enthalpy. Steam and CO_2 escape along faults from deep seated geothermal reservoirs and rise towards the surface. Along this path, steam mostly condenses by cooling, whereas CO_2, being an uncondensable gas, reaches more easily the surface, although it may partially dissolve into shallow aquifers. In geothermal areas, zones characterized by anomalously high soil CO_2 flux, frequently with an elliptical or elongated shape, indicate the presence of faults along which the gas escapes to the surface from the geothermal reservoir (Barberi et al., 2013).

A general soil CO_2 flux survey, carried out in the study area in 2011, with 1336 measurement points over a surface of 12.6 km^2, found CO_2 flux values from 5.2 to 30.250 $g \cdot m^{-2} \cdot d^{-1}$ and showed that anomalous degassing occurs only in the *Solfanare* area, near the natural gas emissions (from about 0.5 km^2) (Carapezza et al., 2015). In the remaining part of the investigated area, soil CO_2 flux values were below the background threshold of 48 $g \cdot m^{-2} \cdot d^{-1}$, and can be attributed to a shallow emission of CO_2 of biological origin generated by the so called "soil respiration" (Carapezza et al., 2015).

As wells demonstrated the presence at depth of an active medium enthalpy geothermal reservoir (Buonasorte et al., 1988), the lack of soil CO_2 anomalous emissions from most of the area indicates the excellent sealing capacity of the flysch and shales cap rock above the reservoir (Carapezza et al., 2015).

In 2013, a seasonal monitoring of soil CO_2 flux was initiated in target areas established around the sites where productive and reinjective wells should be drilled in the future. The aim was to establish the level of the natural degassing of each area, to be able to recognize any possible anomalous gas emission produced by the industrial activity, particularly by the drilling and management of the future wells. We remind that by law, pilot plants must be at zero fluid emissions.

Monitoring began in April 2013 around the wells planned for Castel Giorgio plant (target areas A2, A4, A14 in Figure 8), and since July 2014 it was extended

to the target areas around the planned wells for Torre Alfina plant (AT0, A1, A7 in Figure 8).

From April 2013 to April 2017, 16 surveys of soil CO_2 flux has been carried out, including the two surveys of 3rd - 4th and 7th - 8th June 2016 made during the seismic sequence. The temporal variation of the mean values of soil CO_2 flux measured in all the target areas, starting from the initial 2011 survey, is shown in Figure 10.

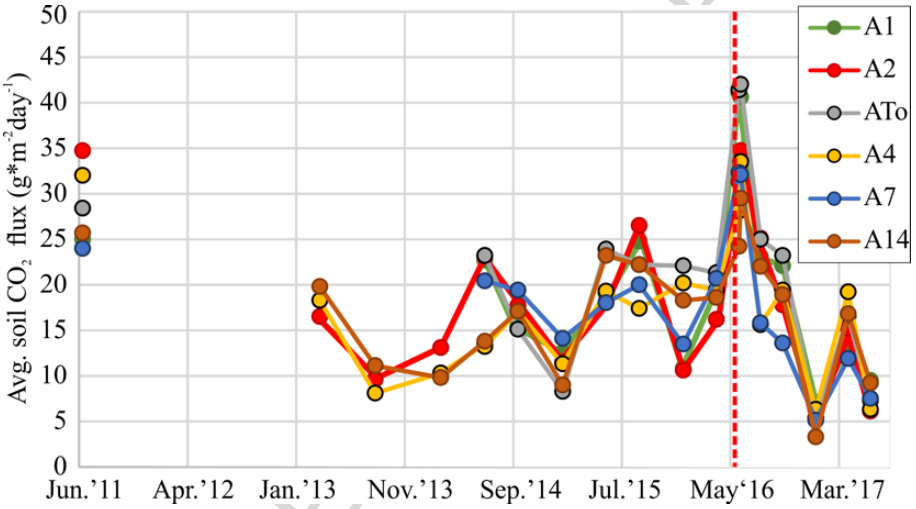

Figure 10: Temporal variation (June '11 - July '17) of the average soil CO_2 fluxes from the target areas of Castel Giorgio -Torre Alfina (see Figure 8 for location). Red dotted vertical line: main shock of the May - June 2016 seismic sequence.

The normal probability plots of the soil CO_2 flux values are reported in Figure 11 and 12 for the surveys carried out in spring-autumn and summer-winter, respectively. The highest values of soil gas flux are recorded in summer, in dry soils with rich vegetation and the lowest values in winter, in often frozen soils.

In almost all surveys, the measured maximum values of soil CO_2 flux are near or slightly above the background threshold of CO_2 flux of biological origin ($48\ g \cdot\ m^{-2} \cdot d^{-1}$). This threshold value has been overpassed, although slightly,

by maximum CO_2 values measured in all target areas (up to a maximum of 112 $g \cdot m^{-2} \cdot d^{-1}$ found in A1 target area) in the surveys carried out on 3rd - 4th and 7th - 8th June 2016, during the seismic sequence. In the A4 target area, soil gas has been sampled on 9th June 2016 at 50 cm depth in the two points (see Figure 8) where the highest values of soil CO_2 flux had been found (82 and 77 $g \cdot m^{-2} \cdot d^{-1}$, respectively). Sampled gas had a CO_2 concentration of 5.20 and 5.06 vol. % respectively. Isotopic analyses of $\delta^{13}C$ of CO_2 gave very negative values (-25.27 and -24.22; see Table 3), with respect to the geothermal gas of *Solfanare* and the reservoir's cap ($\delta^{13}C$ of CO_2 1.2 - 1.4, Table 3), confirming the biological origin of the emitted gas.

In the *Solfanare* area, seismic shaking produced, on 1st June 2016, a significant increase of the maximum and mean value of soil CO_2 flux with respect to those found in the 2011 survey (Table 4). Only after 8 days, soil gas flux had decreased to values lower than in 2011 (Table 4), possibly because the soil was wet due to recent rainfalls.

Date	Area	Measur.	Min.	Max	Avg.
	m^2	no.	$g \cdot m^{-2} d^{-1}$	$g \cdot m^{-2} d^{-1}$	$g \cdot m^{-2} d^{-1}$
May 2011	109000	46	15.3	13244	742.1
1st June 2016	109000	46	14.0	20215	1030.3
9th June 2016	109000	46	12.3	3517	422.0

Table 4: CO_2 flux measurements in the *Solfanare* area.

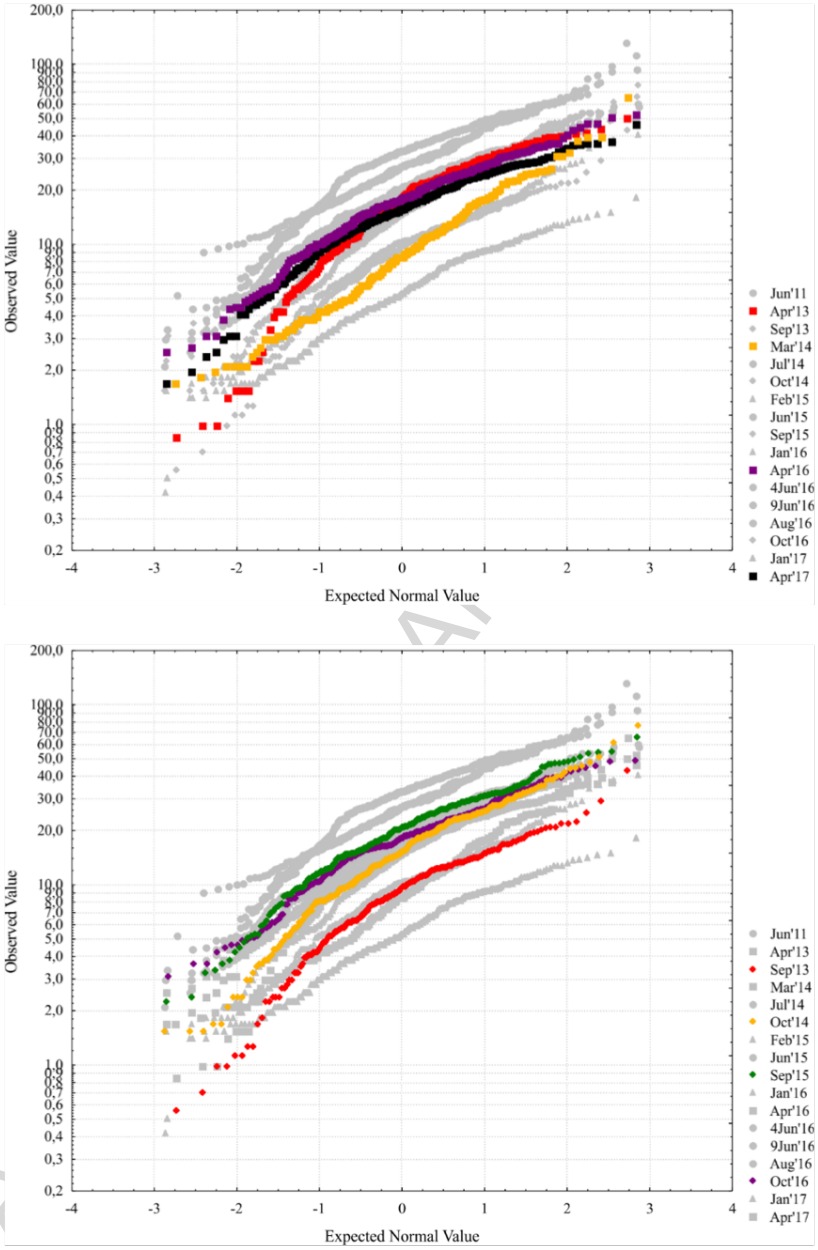

Figure 11: Normal probability plot of soil CO_2 flux values measured in the Castel Giorgio-Torre Alfina target areas from 2011 to 2017. Coloured symbols in the upper and lower panels refer to spring (March - May) and autumn (September - November), respectively.

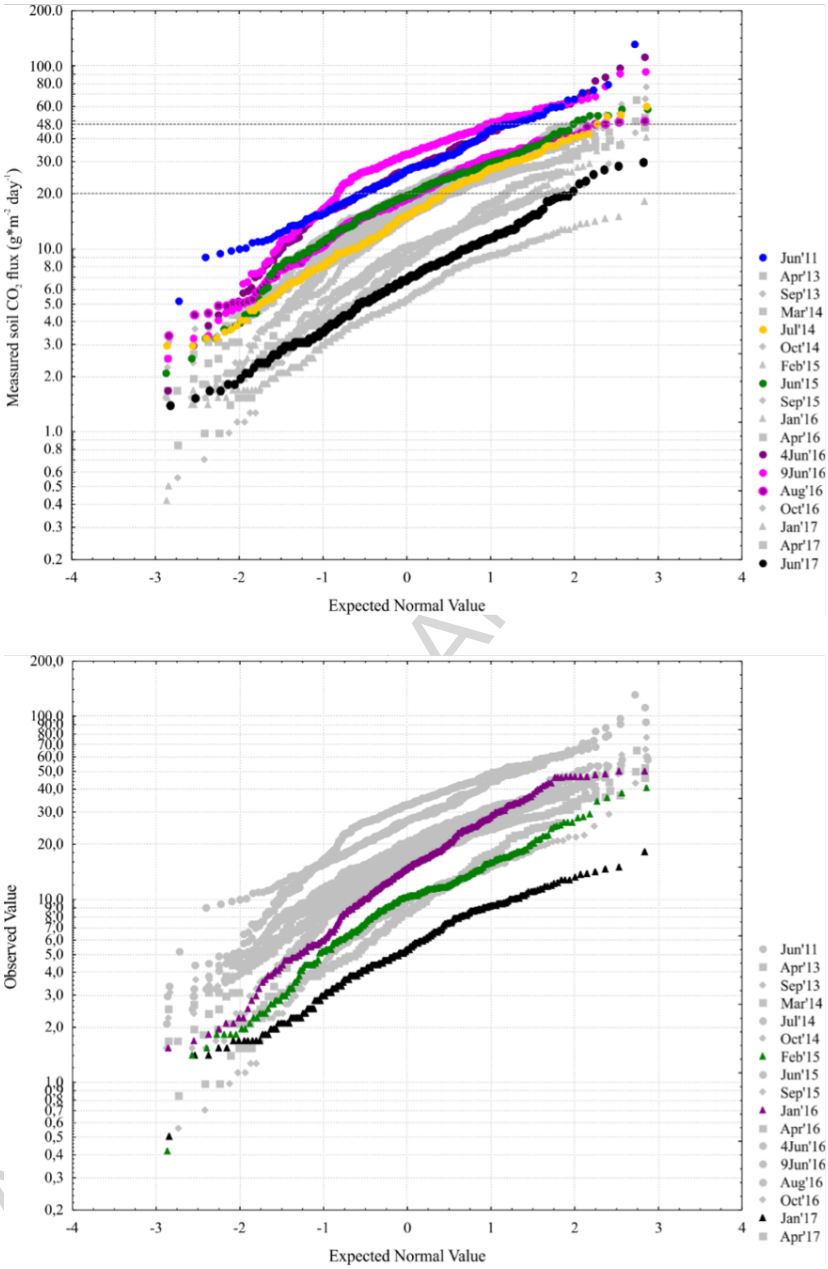

Figure 12: Normal probability plot of soil CO_2 flux values measured in the Castel Giorgio - Torre Alfina target areas from 2011 to 2017. Coloured symbols in the upper and lower panels refer to summer (June - August) and winter (December - February), respectively.

6. The M_e 4.9 earthquake of 6th December 1957

The 6th December 1957 earthquake (M_e 4.9) mainly struck the northeastern sector of the Bolsena lake. From the macroseismic study of ENEL (1995), the maximum intensity degree (I_{max} VII − VIII MCS) was assigned to Castel Giorgio, and the damaged area ($I_o \geq$ VI) includes all villages within 15 km of distance from Castel Giorgio, along a NW-SE oriented hypothetic axis (Figure 13).

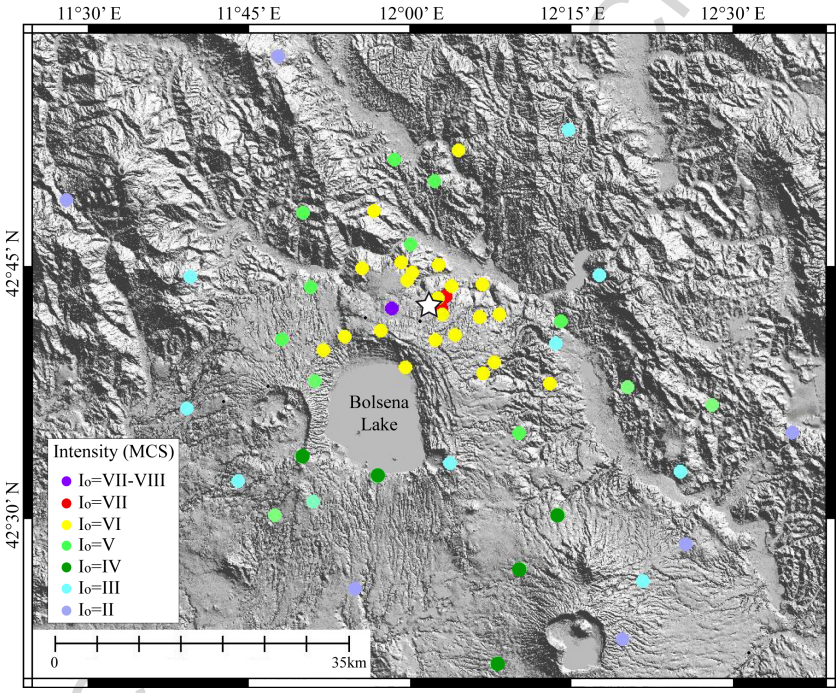

Figure 13: Map of the macroseismic effects of the 6th December 1957 earthquake (after Rovida et al., 2016).

The seismic activity continued until 10th December 1957 with a series of aftershocks, showing a westward migration of the epicentres towards the villages of Torre Alfina and Acquapendente (De Panfilis, 1959). This epicentral area coincides mostly with the geothermal area of Torre Alfina - Castel Giorgio; moreover, the macroseismic epicentre and the temporary evolution of the 1957

seismic sequence are similar to those of May - June 2016. To investigate a possible relationship between these two seismic sequences, we attempted to locate the 1957 earthquake using the arrival times reported in coeval seismic bulletins.

Following the approach of Caciagli et al. (2015) for the location of historical earthquakes, three different sets of theoretical expected arrival times have been computed, by using the AK135 velocity model (Kennett et al., 1995), assuming fixed macroseismic epicentral coordinates (Rovida et al., 2016) and testing different hypocentral depths (5, 10, 20 km). The comparison allows to check the accuracy of the timing reported in the historical bulletins and to correct possible macroscopic inconsistencies, such as misidentification of the seismic phases, large clock bias or typos.

Furthermore, this comparison associates the seismic phases of the historical onset data, according to the IASPEI91 codification (Kennett and Engdahl, 1991). The main source of arrival time data for the 1957 earthquake is the monthly Italian seismic bulletin published by the Italian National Institute of Geophysics (ING) (Caloi, 1958). To integrate the available onset data, a search of coeval seismic bulletins of Euro-mediterranean observatories was performed through the consultation of the on-line bulletin databases compiled in the framework of the EUROSEISMOS project (Ferrari and Pino, 2003) and the ISC-GEM project (Storchak et al., 2013). Both databases are available through the INGV-SISMOS website (http://sismos.rm.ingv.it/en/; Michelini et al., 2005).

From the collected data, we selected 25 onset phases from 13 European observatories (ES-Table 7). For the relocation we used HYPOSAT (Schweitzer, 2001), a routine that allows to invert also traveltime differences, which depend only on the epicentral distance and not on the source time or on systematic timing errors. For these reasons, HYPOSAT turned out to be particularly suitable for historical datasets in case of erroneous absolute timing. Furthermore, for reflected phases, the travel-time difference for a direct phase is strongly influenced by the source depth. To estimate station corrections we adopted the CRUST5.1 model (Mooney et al., 1998).

Origin time (GMT) (hh:mm:ss.ss):	04:54:32.086 ± 0.663
Latitude (°N):	42.759 ± 0.034
Longitude (°E):	12.018 ± 0.080
Depth Z (km):	13.25 ± 3.38
Root mean square (s):	0.555

Table 5: Hypocentral parameters obtained in this study for 6th December 1957 seismic event.

The obtained hypocentre (Table 5) is located close to the village of Castel Viscardo (Figure 3), ca. 7 km north of Castel Giorgio, at a depth of 13.25 km (± 3.38 km) with a mean residual error (rms) of 0.555 s (the complete parameter set is reported in the ES-Table 8).

7. Discussion and conclusions

7.1. Comparison with previous seismicity

In the area of Torre Alfina - Castel Giorgio, the microseismicity recorded by ReMoTA, after its installation in 2014, resulted to be unexpectedly high with 846 seismic events recorded in 24 months in a magnitude range of M_d 0.1 to M_L 2.8, and a depth range of 2 to 8 km (Figure 14, Lisi et al., 2018). More than half of these events occurred in six clusters, lasting a few days each (Table 6) and this is typical swarm behavior of volcanic regions. Figure 14 shows the map and the cross section (SW - NE and NW - SE) for the seismicity clusters.

Comparison of the seismic sequence of May - June 2016 (Figure 4) with the previous recorded by ReMoTA (Figure 14; Lisi et al., 2018) evidences that the May - June 2016 sequence reactivated most of the previously identified structures. In particular, the Castel Giorgio cluster involves the same structure as during the seismic sequence of December 2014 (Table 6). As shown in the profiles of Figure 4 and 14, the hypocentre distribution seems to depict a normal fault (probably structured in two different splays and with smaller right-lateral strike component), NE - SW oriented and SSE-dipping. The epicentral area of the small cluster north of San Lorenzo Nuovo (Figure 4) is coincident with

the clusters recorded in February and April 2016 (Figure 14). The hypocentral distribution of these clusters depict a fault NE-SW oriented and SE-dipping.

The hypocentral solution obtained for the 1957 earthquake is compatible with the damage scenario resulting from the macro-seismic study (ENEL, 1995) and the low RMS residual permits to consider it as a robust solution. Even if - due to the data quality of the 1950s - it cannot be proved with absolute certainty that the seismic source of 1957 is exactly the same as the main shock of the May/June 2016 seismic sequence, it very likely occurred on the same fault system, which is responsible for the major stress release in the study area. This is also in accordance with the temporary evolution described by De Panfilis (1959), who reported during the 1957 seismic sequence the main shock close to Castel Giorgio and the strongest aftershock close to Acquapendente, similarly to what has been observed during the 2016 seismic swarm.

period	color in Fig. 14	n^o of events	Max. magnitude
Nov 13 - 14, 2014	purple	30	$M_d = 1.7$
Dec 21 - 26, 2014	red	158	$M_L = 2.6$
Mar 24 - 28, 2015	orange	53	$M_d = 1.7$
Nov 23 - 29, 2015	light blue	80	$M_d = 1.9$
Feb 28 - Mar 2, 2016	blue	115	$M_d = 1.9$
April 18 - 22, 2016	green	76	$M_d = 2.3$

Table 6: Time, number of events and maximum magnitude of the six major seismic sequences recorded between November 2014 and April 2016.

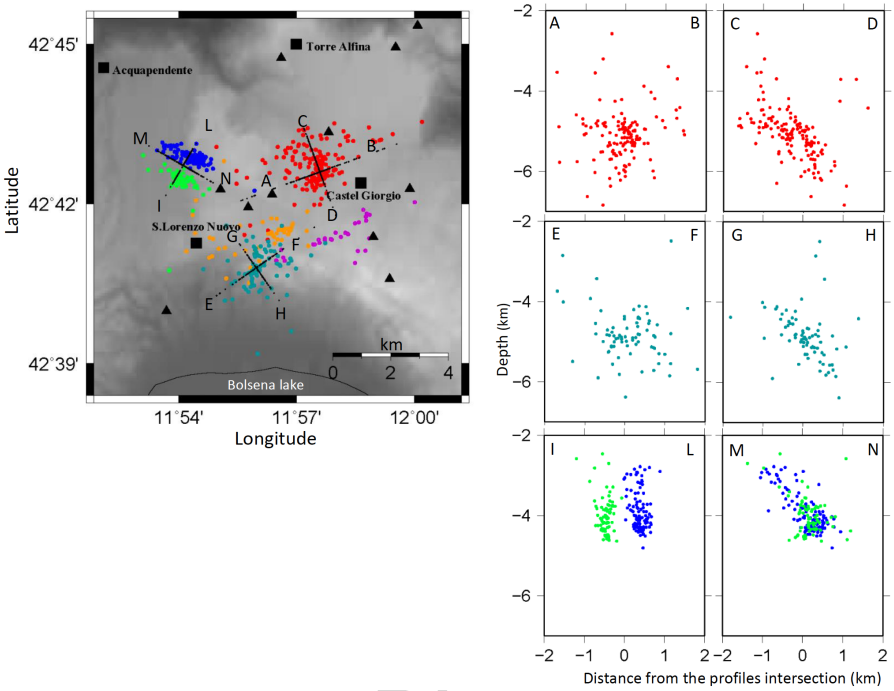

Figure 14: (a) Map of the seismicity clusters recorded by ReMoTA and respective cross sections - along the directions indicated by capital letters - for the main four clusters of December 2014 (red), November 2015 (light blue), February (blue) and April 2016 (green); (modified from Lisi et al., 2018).

7.2. Geochemical observations on the emitted gas

Only minor geochemical variations have been observed on the emitted gas during the seismic sequence of May - June 2016 with respect to data collected before. Basically, no significant changes have been observed in the chemical and isotopic composition of the *Solfanare* gas that has the same composition of that contained in the Torre Alfina geothermal reservoir (Carapezza et al., 2015).

In the final part of the seismic sequence, the use of a continuous CMS, analysing the chemical composition of the *Solfanare* gas with a sampling interval of 30 s, allowed to recognize rapid compositional fluctuations with a general, although weak, decrease in the concentration of reduced species that reached

their minimum values. These short living variations terminated on 9th June 2016, at the end of the seismic sequence.

Data indicate that the steady-state of *Solfanare* degassing was slightly perturbated during the 2016 earthquakes mostly because of recurrent more oxidizing conditions. However, there is no geochemical evidence for an increasing output of deep originated gas.

The repetition of soil CO_2 flux measurements in the target areas that had been previously extensively monitored, and on the *Solfanare* area, shows clearly a general although slight increase in soil gas release produced by the earthquake ground shaking. As a matter of fact, on all target areas the highest mean and maximum CO_2 flux values have been recorded in the surveys carried out on 4th and 9th June 2016, during the final part of the seismic sequence (up to a maximum of 112 g $\cdot\, m^{-2} \cdot d^{-1}$). These relatively low anomalies in the soil gas flux values and the strongly negative $\delta^{13}C_{CO_2}$ isotopic composition of the gas (-25 ‰ vs. PDB, Table 3) confirm that the emitted gas had a shallow organic origin (by soil respiration) and therefore there is no geochemical evidence that new faults emitting deep originated gas have been generated by the 2016 seismic swarm.

7.3. Conclusive remarks

All the earthquakes of the May - June 2016 sequence occurred in the DE and mostly inside the DI. The seismicity is concentrated principally in a deeper range between 3 - 7 km, just beneath the geothermal field, but just above the main shock. An overview of the epicentral distribution of the different clusters recorded since 2014, highlights that the active tectonic structures are orientated principally along the NE - SW and WNW-ESE directions. Hence, the main active structures are neither the faults orientated in direction of the Apennines nor the NNW - SSE oriented structures, such as the *Solfanare* fault.

Noteworthy are the discrepancies between the focal mechanisms of the main shock found by (a) the standard MT, (b) the inversion of the first motion polarities, and (c) the inversion of the full MT. All the routinely calculated MT were

fixed at a depth of 5 km and show a normal fault mechanism with Apenninic strike (Figure 1). We based the inversion of the P-phase polarities on a slightly greater hypocentral depth of 6.7 km (Table 1) and obtained a significant strike-slip component leading to an oblique mechanism (Figure 4). The greater depth resulting from hypocentral determination (see section 1), is further confirmed independently by the depth phase modeling of seismic array data (Figure 6) and is therefore more realistic than the standard depth of 5 km.
The gray line in Figure 5 (a) shows the misfit of the DC source model for different depths. The observation that the misfit becomes abruptly worse below 5 km explains why all the standard MTs had been fixed at 5 km and explains further that the inversion of the first motion polarities compensates the forcing on a double couple solution by introducing a strike slip component. As confirmed by the low misfit, the isotropic component of 25 % and a CLVD of 12.7 % explain those parts that cannot be constrained on a DC solution.

From the HypoDD solutions and the full MT inversion (Figure 5) we conclude that the main shock occurred at a depth of 6.7 km on a fault plane described by strike 101, dip 46, rake -111.

All the seismicity of the May - June 2016 sequence is located above the M_L4.1 main event and is distributed on small distinct faults (such as at San Lorenzo Nuovo, Acquapendente, etc.) and have been triggered by the main shock.

The source mechanism provided by the full moment tensor indicates that rupture processes at depth probably deviate from a pure normal fault. The significant contribution of CLVD and isotropic components suggest a possible opening of fluid cracks below the geothermal reservoir hosted in fractured Mesozoic limestones.

The described seismo-tectonic scenario indicates that the *Solfanare* fault was not activated, being in agreement with the observation that no significant changes have been observed in the chemical and isotopic composition of the *Solfanare* gas. Kinematics and orientation of the activated principal and secondary faults suggest a relationship with the Bolsena caldera collapse (Acocella et al., 2012).

8. Acknowledgements

The present study on Torre Alfina geothermal field have been carried out in the framework of a research contract between INGV and ITW & LKW Geotermia Italia spa. The research was co-financed by Project INGV - DPC 2014 - S2. Data and metadata accessed via FDSN web services at the INGV repository.

9. References

Acocella, V., Palladino, D., Cioni, R., Russo, P., Simei, S., 2012. Caldera structure, amount of collapse, and erupted volumes: The case of Bolsena caldera, Italy. GSA Bulletin 124. doi:10.1130/B30662.1.

Arcoraci, L., Battelli, P., Castellano, C., Marchetti, A., Mele, F., Nardi, A., Pirro, M., Rossi, A., 2012. Bollettino sismico italiano 2009. Quaderni di Geofisica , 52ISSN 1590-2595.

Barberi, F., Carapezza, M., Cioni, R., Lelli, M., Menichini, M., Ranaldi, M., Ricci, T., Tarchini, L., 2013. New geochemical investigations in Platanares and Azacualpa geothermal sites (Honduras). J. Volcanol. Geotherm. Res. 257, 113 – 134.

Batini, F., Bufe, C., Cameli, G., Console, R., Fiordelisi, A., 1980a. Seismic monitoring in Italian geothermal areas I: seismic activity in the Larderello-Travale region., in: Report LBL - 11555 Lawrence Berkeley Laboratory (Ed.), Proceedings Second DOE-ENEL Workshop on Cooperative Research in Geothermal Energy, Berkeley, CA, USA. pp. 20 – 47.

Batini, F., Cameli, G., Carabelli, E., Fiordelisi, A., 1980b. Seismic monitoring in Italian geothermal areas II: seismic activity in the geothermal fields during exploitation, in: Report LBL - 11555 Lawrence Berkeley Laboratory (Ed.), Proceedings Second DOE-ENEL Workshop on Cooperative Research in Geothermal Energy, Berkeley, CA, USA. pp. 48 – 85.

Batini, F., Console, R., Luongo, G., 1985. Seismological study of Larderello-Travale geothermal area. Geothermics 14, 255 – 272.

Batini, F., Fiordelisi, A., Moia, F., 1990. Main features of the seismicity in the Monte Amiata and Latera geothermal areas (Italy), in: Abstracts XXII General Assembly European Seismological Commission, Barcelona, Spain. pp. 649–654.

Braun, T., Cesca, S., Kühn, D., Martirosian-Janssen, A., Dahm, T., 2018. Anthropogenic seismicity in Italy and its relation to tectonics: State of the art and perspectives. Anthropocene 21, 80 – 94. doi:10.1016/j.ancene.2018.02.001.

Braun, T., Dahm, T., Krüger, F., Ohrnberger, M., 2016. Does geothermal exploitation trigger earthquakes in Tuscany? Eos 97. doi:10.1029/2016EO053197.

Braun, T., Pagliuca, N., Gattuso, A., Mele, G., Caciagli, M., Famiani, D., Marchetti, A., Badiali, L., Frepoli, A., Lisi, A., Carapezza, M., 2017. Installazione della rete di monitoraggio sismico remota nell'area geotermica di torre alfina-castel giorgio (lazio settentrionale-umbria). Rapp. Tec. INGV , 1 – 44,URL: www.ingv.it/editoria/rapporti/2017/rapporto370/. ISSN 2039-7941.

Buonasorte, G., Cataldi, R., Ceccarelli, A., Costantini, A., D'Offizi, S., Lazzarotto, A., 1988. Ricerca ed esplorazione nell'area geotermica di Torre Alfina (Lazio-Umbria). Boll. Soc. Geol. It. 107, 265 – 337.

Buonasorte, G., Enrico, P., Adolfo, F., 1991. The alfina 15 well: deep geological data from northern Latium/Torre Alfina geothermal area. Bollettino della Societá Geologica Italiana 110, 823–831.

Caciagli, M., Camassi, R., Danesi, S., Pondrelli, S., Salimbeni, S., 2015. Can we consider the 1951 Caviaga (Northern Italy) earthquakes as non-induced events? Seismol. Res. Lett. 86, 10pp. doi:10.1785/0220150001.

Caloi, P., 1958. Bollettino Sismico Mensile: Dicembre 1957. Technical Report. Istituto Nazionale di Geofisica. Roma. 7 pp, (in italian).

Carapezza, M., Ranaldi, M., Gattuso, A., Pagliuca, N., Tarchini, L., 2015. The sealing capacity of the cap rock above the Torre Alfina geothermal reservoir (Central Italy) revealed by soil co_2 flux investigations. J. Volcanol. Geotherm. Res. 291, 25 – 34. doi:10.1016/j.jvolgeores.2014.12.011.

Cesca, S., Dost, B., Oth, A., 2013. Preface to "triggered and induced seismicity: probabilities and discrimination". J. Seismol. doi:10.1007/s10950-012-9338-z.

Cesca, S., Heimann, S., Stammler, K., Dahm, T., 2010. Automated procedure for point and kinematic source inversion at regional distances. J. Geophys. Res. 115. doi:10.1029/2009JB006450.

Chatelain, J., 1978. Étude fine de la sismicité en zone de collision a l'aide d'un réseau de stations portables: la region Hindu – Kush – Pamir. Ph.D. thesis. Université Paul Sabatier. Toulouse.

Chiarabba, C., Amato, A., Fiordelisi, A., 1995. Upper crustal tomographic images of the Amiata - Vulsini geothermal region, central Italy. J. Geophys. Res. 100, 4953 – 4066.

De Panfilis, M., 1959. Attivitá sismica in Italia dal 1953 al 1957. Ann. of Geophys. 12, 23–148. doi:10.4401/ag-5513. ISSN 2037-416X.

Dialuce, G., Chiarabba, C., DiBucci, D., Doglioni, C., Gasparini, P., Lanari, R., Priolo, E., Zollo, A., 2014. Indirizzi e linee guida per il monitoraggio della sismicitá, delle deformazioni del suolo e delle pressioni di poro nell'ambito delle attivitá antropiche. GdL MISE. Roma. URL: unmig.mise.gov.it/unmig/agenda/upload/85_238.pdf.

Duchi, V., Minissale, A., Ortino, S., Romani, L., 1987. Geothermal prospecting by geochemical methods on natural gas and water discharges in the Vulsini Mts. volcanic district (Central Italy). Geothermics 16, 147 – 157.

ENEL, 1995. Ricerche sui terremoti dell'area di Latera (VT). Internal Report. IRRS-OGSM. Milano-Macerata. 274 pp.

Evans, K., Zappone, A., Kraft, T., Deichmann, N., Moia, F., 2012. A survey of the induced seismic responses to fluid injection in geothermal and CO_2 reservoirs in Europe. Geothermics 41, 30–54.

Ferrari, G., Pino, N., 2003. Euroseismos 2002 – 2003 a project for saving and studying historical seismograms in the euro-mediterranean area, in: Geophys Res Abstr 5, EGS - AGU - EUG Joint Assembly, EGU, Nice, France. 6 - 11 April 2003.

Gutenberg, B., Richter, C., 1954. Seismicity of the Earth and associated phenomena. volume Second edition. Princeton University Press, New Jersey. 310 pp.

Herrmann, R., Malagnini, L., Munafó, I., 2011. Regional moment tensors of the 2009 l'Aquila earthquake sequence. Bull. Seism. Soc. Am. 101, 975 – 993. URL: eqinfo.eas.slu.edu/eqc/eqc_mt/MECH.IT/, doi:10.1785/0120100184.

Hudson, J., Pearce, R., Rogers, R., 1989. Source type plot inversion of the moment tensor. J. Geophys. Res. 94, 765 – 774.

Hutton, J., Boore, M., 1987. The M_L scale in southern California. Bull. Seis. Soc. Am. 77, 2074 – 2094.

ISIDe working group, 2016. Italian seismological instrumental and parametric database, version 1.0. doi:10.13127/ISIDe10.13127/ISIDe.

Kennett, B., Engdahl, E., 1991. Traveltimes for global earthquake location and phase identification. Geophys. J. Int. 105, 429–465.

Kennett, B., Engdahl, E., Buland, R., 1995. Constraints on seismic velocities in the earth from traveltimes,. Geophys. J. Int. 122, 108 – 124.

Lahr, J., 1999. HYPOELLIPSE: a computer program for determining local earthquake hypocentral parameters, magnitude, and first-motion pattern. Open-File Report 99âĂŞ23. US Geological Survey. Version 1.1, 119 pp.

Lisi, A., Badiali, L., Caciagli, M., Carapezza, M., Famiani, D., Frepoli, A., Gattuso, A., Marchetti, A., Mele, G., Pagliuca, N., Braun, T., 2018. Zero

level seismicity recorded in the area of the future geothermal production sites of Castel Giorgio and Torre Alfina (Italy). Ann. of Geophys. submitted.

Locati, M., Camassi, R., Rovida, A., Ercolani, E., Bernardini, F., Castelli, V., Caracciolo, C., Tertulliani, A., Rossi, A., Azzaro, R., D'Amico, S., Conte, S., Rocchetti, E., 2016. DBMI15, the 2015 version of the Italian Macroseismic Database. Technical Report. Istituto Nazionale di Geofisica e Vulcanologia. doi:10.6092/INGV.IT-DBMI15.

Martelli, M., 2002. Crust-mantle interaction along the Italian peninsula: inferences from He isotope geochemistry in free gases and fluid inclusions. Ph.D. thesis. University of Palermo.

Martelli, M., Nuccio, P., Stuart, F., Burgess, R., Ellam, R., Italiano, F., 2004. Helium-strontium isotope constraints on mantle evolution beneath the Roman comagmatic province, Italy. Earth Planet. Sci. Lett. 224, 295–308.

Mele, F., Arcoraci, L., Battelli, P., Berardi, M., Castellano, C., Lozzi, G., Marchetti, A., Nardi, A., Pirro, M., A., R., 2010. Bollettino Sismico Italiano 2008, in: Quaderni di Geofisica. INGV. volume 85.

Michelini, A., De Simoni, B., Amato, A., Boschi, E., 2005. Collecting, digitizing, and distributing historical seismological data. Eos, Trans. AGU 86, 261 – 266.

Moia, F., Angeloni, P., Cameli, G., Zaninetti, A., 1993. Monitoring induced seismicity around geothermal fields and reservoirs, in: First Egyptian Conference on Earthquake Engineering, Hurgada – Egypt, pp. 1–10.

Mooney, W., Laske, G., Masters, T., 1998. Crust 5.1: A global crustal model at 5° x 5°. J. Geophys. Res. 103, 727–747. Solid Earth.

Mucciarelli, M., Gallipoli, M., Fiaschi, A., Pratesi, G., 2001. Osservazioni sul danneggiamento nella zona del Monte Amiata a seguito dell'evento del 1 Aprile 2000, in: X Congresso Nazionale "L'ingegneria Sismica in Italia", Potenza-Matera. p. 9.

Pondrelli, S., Salimbeni, S., Ekström, G., Morelli, A., Gasperini, P., Vannucci, G., 2006. The italian cmt dataset from 1977 to the present. Phys. Earth Planet. Int. 159, 286–303. URL: autorcmt.bo.ingv.it/QRCMT-on-line/, doi:10.1016/j.pepi.2006.07.008.

Pontoise, B., Monfret, T., 2004. Shallow seismogenic zone detected from an o shore-onshore temporary seismic network in the Esmeraldas area (northern Ecuador). Geochemistry, Geophysics, Geosystems 5, 22. doi:10.1029/2003GC000561. aGU and the Geochemical Society.

Rovida, A., Locati, M., Camassi, R., Lolli, B., (eds), P.G., 2016. CPTI15, the 2015 version of the Parametric Catalogue of Italian Earthquakes. Technical Report. Istituto Nazionale di Geofisica e Vulcanologia. URL: http://emidius.mi.ingv.it/CPTI15-DBMI15/query_place/, doi:10.6092/INGV.IT-CPTI15.

Schweitzer, J., 2001. Hyposat – an enhanced routine to locate seismic events. Pure Appl. Geophys. 158, 277–289. doi:10.1007/PL00001160.

Scognamiglio, L., Tinti, E., Michelini, A., 2009. Real-time determination of seismic moment tensor for the italian region. Bull. Seis. Soc. Am. 99, 2223–2242. URL: cnt.rm.ingv.it/tdmt.

Storchak, D., Di Giacomo, D., Bondár, I., Engdahl, E.R., Harris, J., Lee, W., or, A.V., Bormann, P., 2013. Public Release of the ISC – GEM – Global Instrumental Earthquake Catalogue (1900 – 2009). Seis. Res. Lett. 84, 810 – 815.

Terlizzese, F., 2016. Linee guida per l'utilizzazione della risorsa geotermica a media e alta entalpia. GdL MISE. Roma. URL: http://unmig.mise.gov.it/unmig/geotermia/lineeguida.pdf.

Volpi, G., Magri, F., Colucci, F., Fischer, T., De Caro, M., Crosta, G., 2018. Modeling highly buoyant flows in the Castel Giorgio: Torre Alfina deep geothermal reservoir. Geofluids , 19pp ,doi:10.1155/2018/3818629.

Waldhauser, F., 2001. HypoDD - A Program to Compute Double-Difference Hypocenter Locations. Open-File Report 01-113. US Geological Survey.

Waldhauser, F., Ellsworth, W., 2000. A double-difference earthquake location algorithm: Method and application to the northern Hayward fault. Bull. Seism. Soc. Am. 90, 1353–1368.

10. Electronic supplement

Station code	Original		Used	
	phase	onset time (hh:mm:ss)	phase	onset time (hh:mm:ss)
ROM	Pg	04:54:50.000	Pn	04:54:50.000
ROM	Sg	04:55:04.000	Sn	04:55:04.000
FIR	Pg	04:54:55.000	Pg	04:54:55.000
FIR	Sg	04:55:13.000	Sn	04:55:13.000
PRT*	P	04:54:56.000	Pn	04:54:56.000
BOL	Pn	04:55:10.500	Pn	04:55:03.500
BOL	Sn	04:55:37.000	Sg	04:55:30.000
PAV	e(Pn)	04:55:34.000	Pg	04:55:34.000
PAV	e	04:56:11.000	Sn	04:56:02.000
MON	ePn	04:55:27.500	Pn	04:55:25.500
MON	ePg	04:55:40.500	Pg	04:55:38.500
ZAG	P	04:55:52.000	Pg	04:55:52.000
ZAG	S	04:56:22.000	Sn	04:56:22.000
BES	ePn	04:56:12.000	Pn	04:56:03.000
BES	eSn	04:56:59.000	Sg	04:57:50.000
STU	eSn	04:57:17.500	Sn	04:57:17.500
STR	eSn	04:57:23.000	Sn	04:57:23.000
GRC	ePn	04:56:28.000	Pn	04:56:25.000
GRC	ePg	04:56:53.000	Sn	04:57:50.000
JEN	e(Pn)	04:56:33.000	Pn	04:56:33.000
JEN	e(Pg)	04:57:14.000	sPg	04:57:14.000
JEN	e(Sn)	04:58:03.000	Sn	04:58:03.000
CLL	S	04:58:12.000	Sn	04:58:12.000
HLE	i	04:59:36.000	Pn	04:56:36.000
HLE	i	04:59:44.000	*PnPn	04:56:44.000

Table 7: Seismic phases used to locate the 6th December 1957 earthquake. * bulletin lacking, onset read from original seismogram.

Source time T_0(GMT)	04:54:32.086
ΔT_0 (s)	0.663
Latitude (°N)	42.759
Δ Latitude (°)	0.034
Longitude (°E)	12.018
Δ Longitude (°)	0.080
Depth Z (km)	13.25
ΔZ(km)	3.38
V_p/V_s	1.74
$\Delta(V_p/V_s)$	0.01
Maximum epicentral error ellipse (km)	6.78
Minimum epicentral error ellipse (km)	6.49
Epicentral error ellipse azimuth (°)	42.6
Root mean square (s)	0.555
n° onset	17
n° travel-time differences	14
Azimuthal gap (°)	131.1

Table 8: (ES): Complete hypocentral parameters set obtained in this study for 6^{th} December 1957 seismic event. For each parameter x, Δx indicates the associated uncertainty.

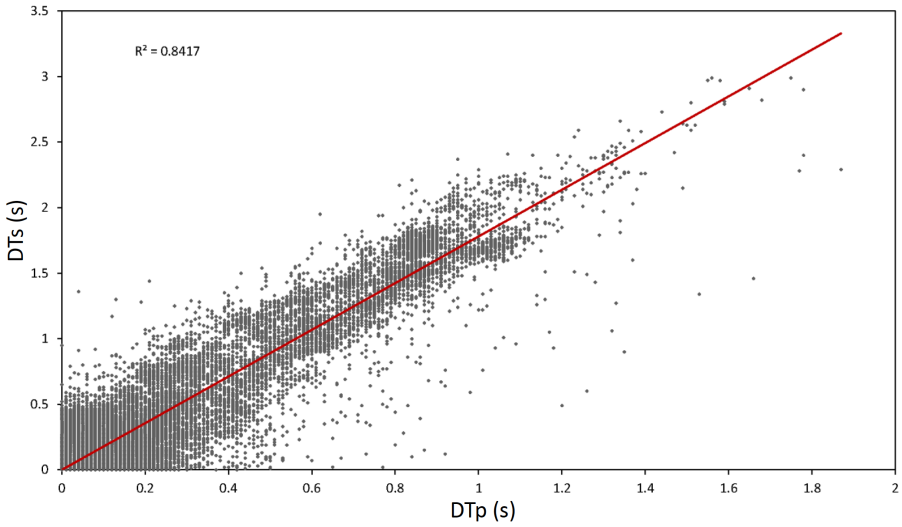

Figure 15: (ES): Wadati diagram. Linear fit of ΔT_s versus ΔT_p (S and P wave differential time measurements, respectively). The V_p/V_s ratio is 1.8167 (RMS = 0.0197, R = 0.84)

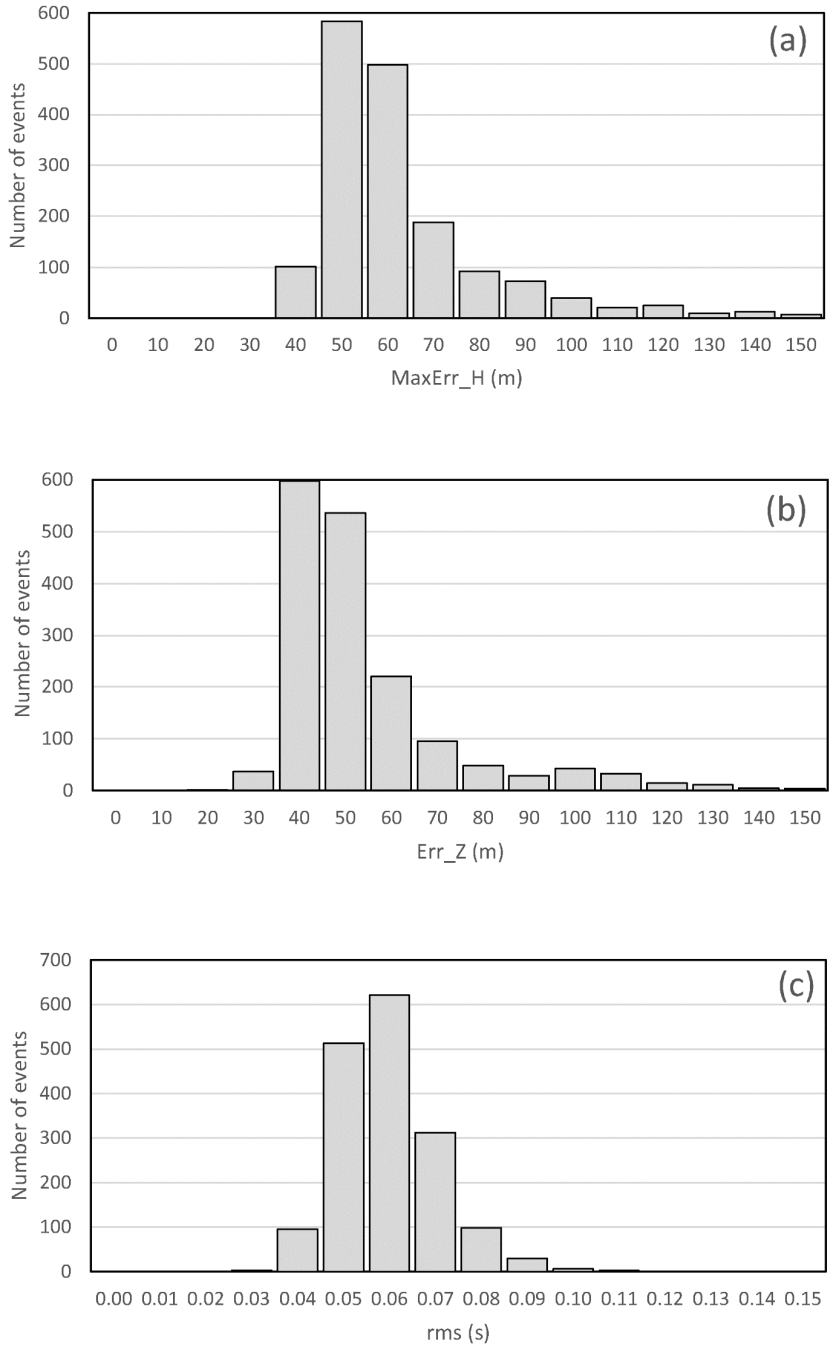

Figure 16: (ES): (a) Horizontal errors, (b) vertical errors, and (c) RMS of the relocated earthquakes occurred from 30th May to 31st December.

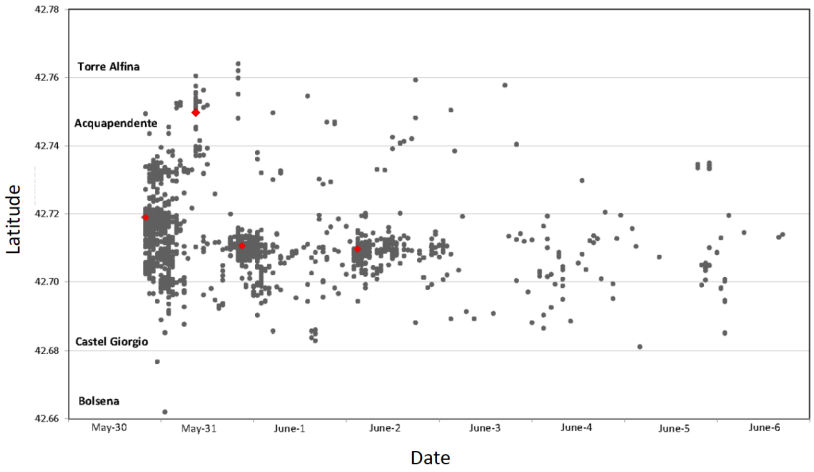

Figure 17: (ES): Spatial and temporal distribution of the seismic sequence from 30$^{\text{th}}$ May to 6$^{\text{th}}$ June. Each event is plotted as a function of latitude and origin time. Red diamonds indicate the earthquakes with $M_L \geq 3$; city names are reported close to their respective latitude.